DOI: https://doi.org/10.14311/TPFM.2026.023

AEROELASTIC RESPONSE AND WAKE ANALYSIS OF A BLADE CASCADE EXPOSED TO CONTROLLED RADIAL CROSS-FLOW

P. Procházka[1], V. Skála[1], P. Šnábl[1], C. S. Prasad[1]

[1] Department of Fluid Dynamics, Institute of Thermomechanics, Czech Academy of Sciences, Dolejškova 5, 182 00 Praha 8, Czech Republic

Abstract

The aeroelastic stability of a blade cascade exposed to a strongly three-dimensional cross-flow field is experimentally investigated. A linear cascade consisting of thirteen flexible NACA 0010 blades is studied in a wind tunnel equipped with a bypass system that introduces a controlled radial velocity component. The influence of cross-flow on blade vibration response and wake topology is examined using time-resolved particle image velocimetry. While the cascade remains stable under purely axial inflow, the introduction of radial cross-flow leads to the onset of self-induced blade oscillations with increasing amplitude. The wake structure transitions from a regular vortex street to a highly three-dimensional and chaotic flow characterized by broadband frequency content. The results highlight the significant role of radial flow in destabilizing blade cascades under off-design operating conditions.

Keywords: aeroelasticity, self-induced flutter, PIV, FFT, bypass

1 Introduction

Steam turbines in thermal power plants were traditionally designed for maximum efficiency at nominal load conditions and still are. However, the electric grid now requires greater controllability as green energy sources grow in share of the energy mix. Power plant operators are compelled to run turbines outside their design conditions, where efficiency drops rapidly, and the risk of flutter increases significantly.

When the power output demand is too low, a reduced mass flow ratio redistributes the pressure field, with a more pronounced radial flow component; the inlet velocity becomes too low, and the relative angle of attack shifts, increasing the risk of stall flutter. This can cause damage or even destruction of the turbine. The last stage of the steam turbine, the low-pressure section, is especially sensitive to flutter because its blades are very long and thin, have a low-camber profile, and feature sharp leading and trailing edges.

The pressure redistribution with spanwise velocity across the blade stage causes two significant vortical structures - one near the blade tip and the other near the blade root, along with a notable backflow region [1]. Consequently, the bladed wheel is subjected to a highly turbulent three-dimensional cross-flow field with a prominent radial flow component.

The aeroelastic stability of the bladed wheel remains a highly challenging research area because it is difficult to model physically. There is a lack of experimental data to validate extensive CFD modeling. Flutter, or even stall flutter, is usually studied experimentally in a planar blade cascade with uniform incoming flow conditions, e.g., [2, 3, 4]. There are also studies focused on annular blade cascades [5], where the flow is inherently three-dimensional. This study aims to investigate how the radial component of velocity affects blade cascade stability and flow structures that could lead to unstable behavior. A key strength of this study is that the radial flow proportion can be controlled with very high precision, as explained in the next chapter.

This paper expands on a previous detailed experimental study of stall flutter in a five-bladed planar cascade under force excitation [6, 7]. In that case, the blades were excited by a force exciter, and the aeroelastic coupling between the blades and the flow field was measured, although the cascade's periodicity was limited. The current study uses blades that are securely fixed to the bottom wall of the test section, with no external excitation; self-induced flutter is triggered. The main goal of this paper is to describe how radial flow affects the wake topology behind the blades and to evaluate the stability of the cascade. This research will help improve the understanding of how energy transfers between the flow and the blade body.

2 Experimental setup

The blade cascade under investigation is composed of 13 blades with a NACA 0010 profile. The chord length c is 100 mm, and the blade solidity is 0.5 (chord-to-chord distance is 50 mm). The blade length is 800 mm; they are fixed from the outside to the bottom wall of the test section. The wetted span is 700 mm. The stagger angle is 90°, which means that the connecting line of the leading edges is perpendicular to the freestream when the angle of attack (AoA) is zero. This incidence angle can be set over a wide range; for this study, a moderate value (AoA = 5°) was investigated. The blade bodies are not rigid; they are flexible because they are made of a carbon fiber composite. The blades are quite stiff yet very light. The properties of each blade are more or less the same (see Table 1). Despite being rigidly mounted to the tunnel facility, the blades exhibit measurable vibrations due to their partial flexibility.

Table 1: The properties of the three middle blades.

Blade No.	-1		0	+1
Eigenfrequency	20.1 Hz		19.7 Hz	19.9 Hz
Mass	159 g		154 g	157 g

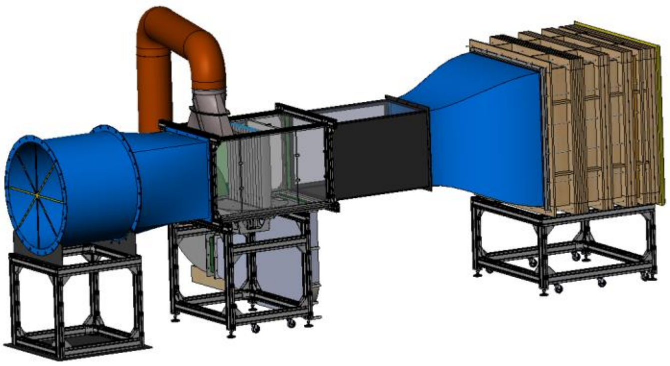

Figure 1: The design of the Eiffel tunnel and the bypass tunnel with circular pipes for the suction part and a rectangular pipe for the blowing; the blade cascade is inside the Perspex test section.

The model of the cascade installed in the test section of the Eiffel tunnel is shown in Figure 1. The cascade is positioned upright. The under-pressure test section measures 700 × 700 mm and is 1200 mm long, with an additional one-meter-long auxiliary passing section included for undisturbed pressure measurements. Before the test section, there is one honeycomb and six fine-mesh screens, which ensure a smooth flow with a low turbulence intensity of 0.5%. The freestream velocity can be adjusted up to 25 m/s.

Generally, there are passive and active approaches to deflect the main tunnel freestream. One can utilize shaping of the test section walls to introduce a spanwise velocity component relative to the cascade or use a shaped mesh screen to generate a velocity profile with a strong gradient. For controlling flow regimes, active methods are highly desirable. Many applications with perpendicular stream blowing into the main freestream are reported [9]. However, such approaches do not influence the flow field throughout the entire cross-section. This research utilizes a unique system that uses a second wind tunnel to produce cross-flow throughout the entire test section via a so-called bypass tunnel. Two rectangular orifices (650 × 100 mm) are integrated into the test section to introduce the radial flow component. Their dimensions and location were designed based on CFD tools. The orifice in front of the cascade is used for blowing, and the one behind the cascade is used for flow suction. Both orifices are connected by pipelines (Fig. 1), and the bypass flow is driven by a radial ventilator. By varying the bypass-to-main flow-rate ratio, the strength of the radial velocity component can be controlled in a well-defined manner. As the bypass flow increases, a more pronounced spanwise component develops upstream of the cascade. An example of the flow deviation (S-shape) is visible in Figure 2, where SAFEX particles were used to seed the flow as smoke lines. The area where the distance between lines decreases is characterized by strong velocity overshoot.

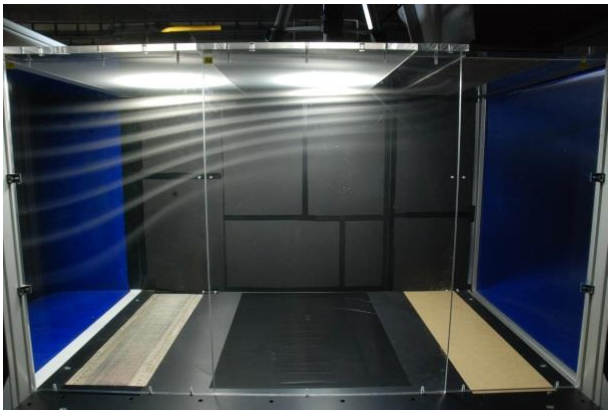

Figure 2: Smoke lines to visualize the effect of bypass cross-flow.

The bypass tunnel was equipped with static pressure sampling to evaluate the volume velocity (and corresponding flow rate), which can differ significantly when the flow conditions in the main tunnel are changed (e.g., varying AoA, different vibration modes, etc.). These pressure sensors were calibrated against the pure outlet flow rate from the blowing orifice using hot-wire anemometry for several bypass-to-main tunnel flow rate ratios. This approach enables the maintenance of high run-to-run repeatability when velocity deviations are constrained to within 1%. Note that the cross-section of the bypass flow is approximately seven times smaller; therefore, higher velocities are often applied in the bypass tunnel than in the main tunnel to introduce a remarkable spanwise velocity component. Six different regimes are presented in this paper to evaluate the wake properties. The main tunnel was set either to 5 or 10 m/s, and the bypass tunnel was turned off or set to 5 or 10 m/s. The corresponding flow rates are shown in Table 2. The Reynolds number based on the blade chord varies from $3 \cdot 10^4$ to $10 \cdot 10^4$.

Table 2. – Flow rates of the main bypass tunnel for six regimes.

main\bypass	0 m/s	5 m/s	10 m/s
5 m/s	2,45m^3/s (R 5 – 0)	2,45 + 0,325m^3/s (R 5 – 5)	2,45 + 0,65m^3/s (R5 – 10)
10 m/s	4,9m^3/s (R 10 – 0)	4,9 + 0,325m^3/s (R 10 – 5)	4,9 + 0,65m^3/s (R10 – 10)

The main goals were to study the wake flow topology and to evaluate the blade vibration response. For both tasks, a fast CMOS camera was used to either acquire blade-tip vibration or track seeding particles in the flow. This camera is part of a time-resolved Particle Image Velocimetry (TR-PIV) system used to acquire and evaluate spatio-temporal velocity fields. The sampling frequency was 1000 Hz, enabling the study of flow fluctuations. Under generally accepted assumptions, the typical uncertainty associated with PIV flow velocity measurement is approximately 2%. For more detailed information about the PIV system and its limits, see reference [8].

3 Results and discussion

The cascade response at the tip of the middle five blades was studied for 21 different flow regimes. Although the cascade demonstrates stable behavior for main-tunnel flow velocities up to 20 m/s, even a small, nonzero bypass value leads to a gradual onset of blade oscillation. The mean oscillation amplitude across the full range of both wind tunnels is shown in Figure 3. In regime R10–10 (Table 2), the mean amplitude is 0.5 mm, the largest measured by PIV, indicating that crossflow promotes greater oscillations. The influence of the main-tunnel velocity is negligible, while the cross-flow accelerates the velocity at the blade tip and promotes the formation of a pronounced recirculation region near the blade root. In addition, the blades in the middle part are surrounded by an airstream with high turbulence intensity and a significant slope. Further in the text, the results evaluated from the TR-PIV method will be discussed. The center of the Cartesian coordinate system for all figures was set to the bottom wall of the tunnel, at the midpoint of the chord of the central blade.

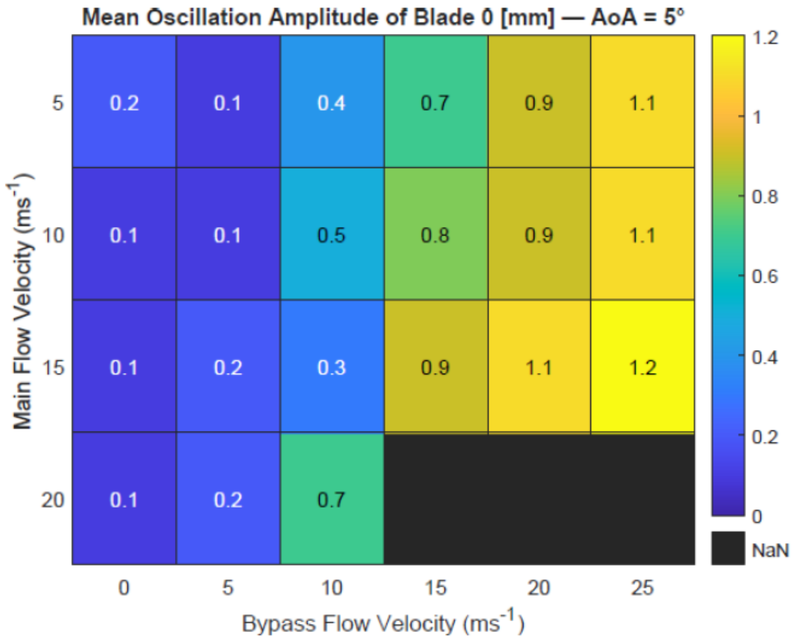

Figure 3: Mean oscillation amplitude of blade 0 for various combinations of main tunnel and bypass tunnel velocities.

To describe the flow topology in front of, between, and behind the blades, velocity vector maps are presented. Black vectors are used to plot the streamwise and spanwise velocity components in the plane of measurement. Vector lines (blue or black) are used to visualize the flow topology caused by the bypass tunnel. The blade bodies are highlighted in black. The vertical plane (x, z) at the center of the test section was acquired to show the S-shape of the cross-flow. Horizontal planes (x, y) were investigated to rigorously study the vortex street in the wake at several locations. Figure 4 compares PIV data and CFD simulation of the vertical mid-plane for three different regimes from the first row of Table 2. The left-hand figure is plotted when no bypass flow is applied. Parallel vectors, oriented perpendicular to the blade span, are distributed across the height of the test section. The other two graphs in Figure 4 show that the radial flow component can be approximately doubled when the bypass flow velocity is increased from 5 to 10 m/s. Similarly, the area of the backflow region can be doubled when using a doubled bypass flow rate. The centers of the recirculation regions are located at approximately 100 mm and 200 mm in height for bypass velocities of 5 m/s and 10 m/s, respectively. An analysis of CFD-calculated data leads to the same conclusions.

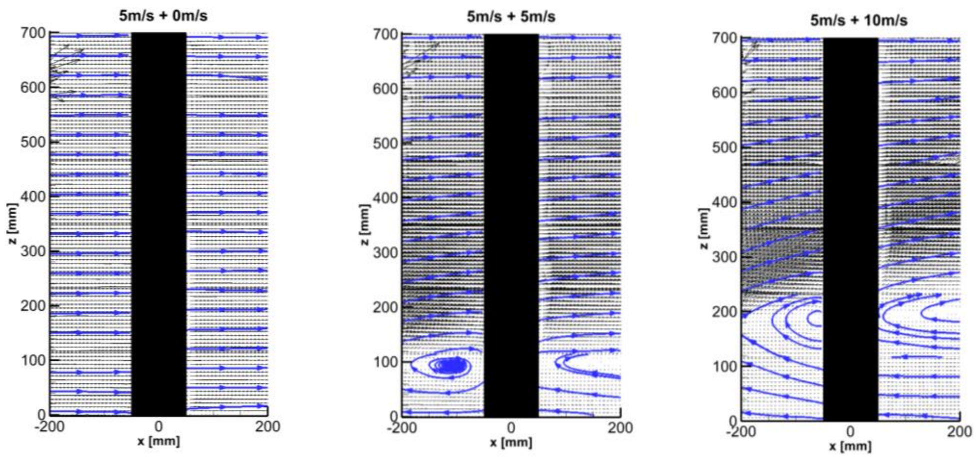

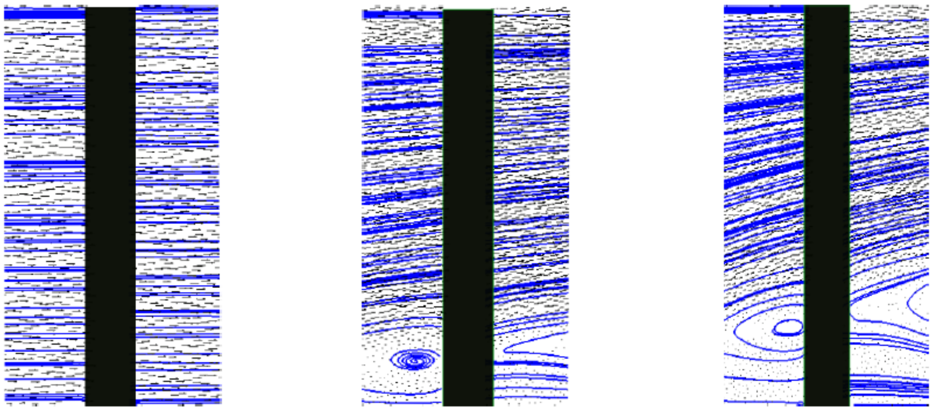

Figure 4: The distribution of velocity vector field in the vertical plane in front and behind the cascade; flow field for incoming flow velocity 5 m/s with no bypass flow (left), bypass flow of 5 m/s (middle), and 10 m/s (right). Lower (CFD) streamline at mid-secession for the same flow conditions.

It becomes apparent that the flow field topology (velocity magnitudes, proportion of the radial component, wake character) is totally different for any horizontal plane perpendicular to the blade bodies. To illustrate this strong three-dimensionality, Figure 5 is plotted for two different horizontal planes. Both are located about 210 mm from the walls – plane 31% is above the bottom of the test section, and plane 70% is located below the ceiling of the tunnel. With the bypass flow turned off, the velocity distribution is identical in both horizontal planes. A bypass flow set to 10 m/s with a main freestream of 5 m/s is capable of changing not only the velocity magnitude distribution, but also the shape of the wakes behind the cascade. Moreover, the flow fluctuation activity (determined by turbulent kinetic energy, TKE) is more than 5 times higher in the plane closest to the tunnel bottom. The main tunnel flow interacts with the bypass flow, leading to highly turbulent, broadband vorticity. In contrast, the flow near the upper part is rather smooth, with a pronounced velocity overshoot. At the lower plane (31%), the time-averaged velocity shows a forward distribution. However, for planes at 10% and 20%, a backward velocity region dominates.

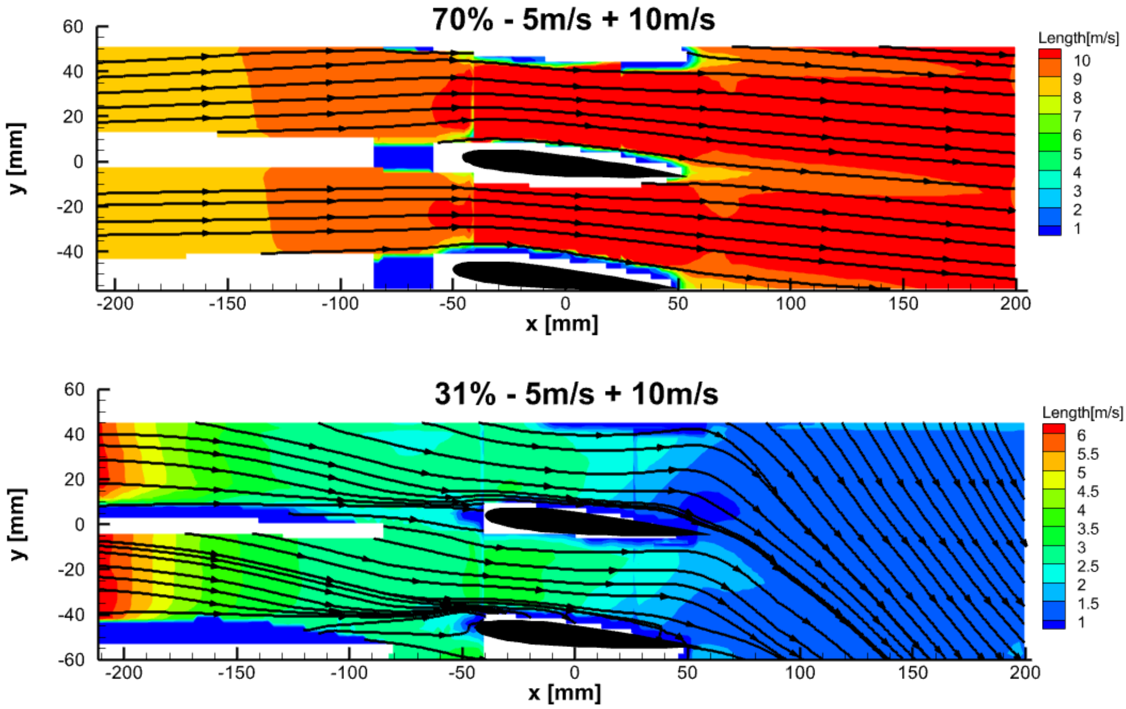

Figure 5: The distribution of velocity magnitude (length) and vector lines in the vicinity of the three middle blades; plane at 70% of the test section - 490 mm above the bottom (upper) and 31% - 217 mm (lower).

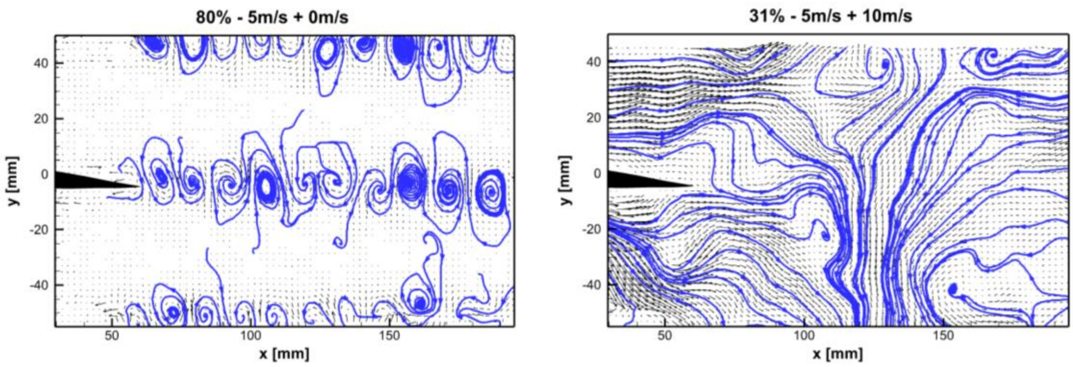

Figure 6: Instantaneous streamlines in the wake of the middle blade at 80% of the test section height (left) and at 31% (right); vortex street and chaotic backflow region.

The organization of the flow can be demonstrated using instantaneous flow fields. A regular vortex street is visible at higher horizontal planes, where the bypass cross-flow causes a velocity overshoot. This vortex street is linked to a significant frequency, as shown in Figure 7. This regular wake pattern is replaced by a chaotic flow region with random forward and backward flow directions at the lower plane (Fig. 6, right), where the blades experience a highly turbulent mixed flow. The FFT analysis cannot identify a strong peak there; instead, it shows a broadband frequency spectrum with several non-dominant peaks.

The FFT analysis was conducted at the same point, 50 mm downstream from the blade's trailing edge, on horizontal planes at 90%, 80%, 70%, 50%, 31%, 20%, and 10%. The spanwise velocity component was included to evaluate the frequency spectra. Four examples of such spectra are plotted in Figure 7. If a pure vortex street is present in the wake, the spectrum shows a sharp peak (Figure 7, lower left corner), highlighted in bold in Table 4. When the bypass significantly influences the wake, this sharp peak is no longer present, as multiple coherent structures with diverse frequencies create the flow field topology.

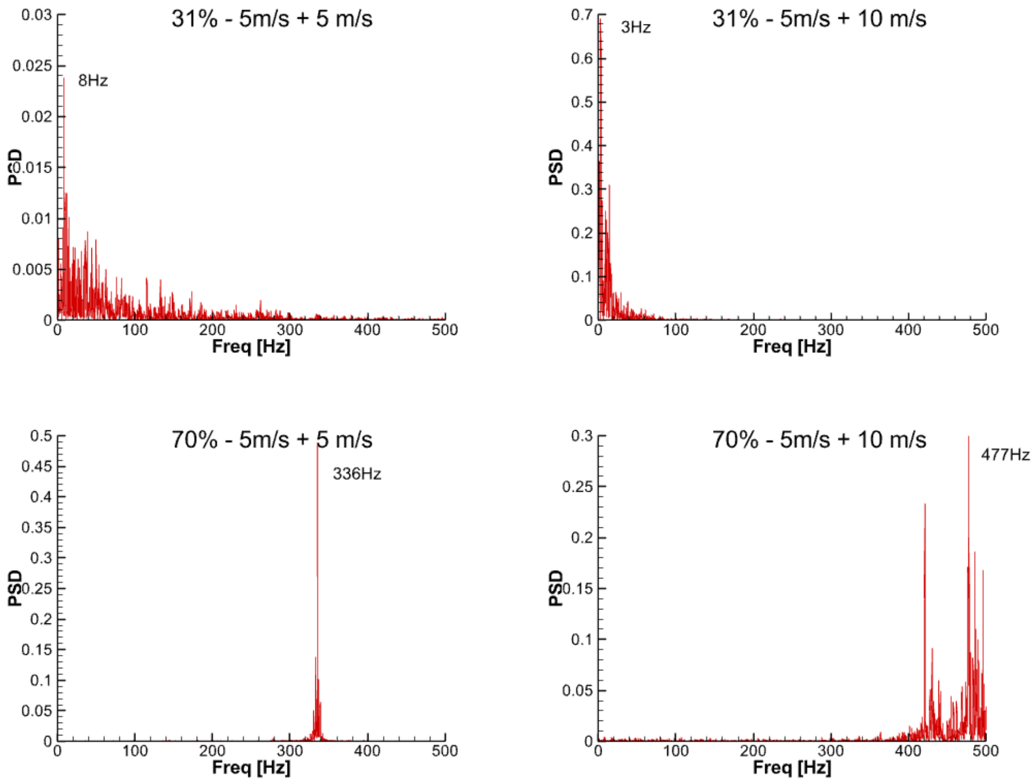

Figure 7: Examples of frequency spectrum evaluated at the point inside the wake of the middle blade; two horizontal planes from Fig. 5 and two bypass regimes are plotted.

Table 3. – The mean velocity magnitude at the wake point for six bypass regimes evaluated at the horizontal plane 90%.

	R 5 - 0	R 10 - 0	R 5 - 5	R 5 - 10	R 10 - 5	R 10 - 10
90%	5.1 m/s	10.4 m/s	6.7 m/s	9.7 m/s	10.8 m/s	14.5 m/s

Table 4. – The highest peak evaluated from frequency spectra; a sharp peak is highlighted in bold.

	R 5 - 0	R 10 - 0	R 5 - 5	R 5 - 10	R 10 - 5	R 10 - 10
90%	**200 Hz**	**448 Hz**	**336 Hz**	**421 Hz**	**423 Hz**	**289 Hz**
80%	**200 Hz**	**448 Hz**	**338 Hz**	**421 Hz**	**423 Hz**	**289 Hz**
70%	**200 Hz**	**448 Hz**	**336 Hz**	477 Hz	**481 Hz**	**289 Hz**
50%	**200 Hz**	471 Hz	**334 Hz**	7 Hz	495 Hz	**289 Hz**
31%	**200 Hz**	**450 Hz**	8 Hz	3 Hz	423 Hz	17 Hz
20%	NA	NA	1 Hz	5 Hz	325 Hz	x
10%	NA	NA	4 Hz	3 Hz	34 Hz	x

The shedding frequency is strongly correlated with the incoming velocity. Table 3 is included to indicate the local velocity at the evaluated wake point and to show how it changes with the applied regime. Although only the uppermost horizontal plane is listed, it indicates that the applied bypass regime accelerates the flow in this region. A higher bypass flow rate results in higher incoming and local velocities. In such a case, the frequency of vortex shedding should exhibit the same trend.

Finally, Table 4 summarizes all frequency peaks evaluated in the wake of the central blade. Note that the first three uppermost planes are characterized exclusively by sharp peak values. These are the planes where the bypass cross-flow has an insufficient effect to break the regularity of the vortex street. Another important conclusion is that without bypass flow, the peak value remains at the same magnitude for both applied main tunnel flow rates. However, at higher flow rates, a limitation of the method becomes apparent, namely undersampling. The acquisition frequency of 1 kHz is insufficient, so it is not possible to estimate the precise frequency peak. This is evident in the last column of the table: although the value is identical across all planes, it is clearly undersampled.

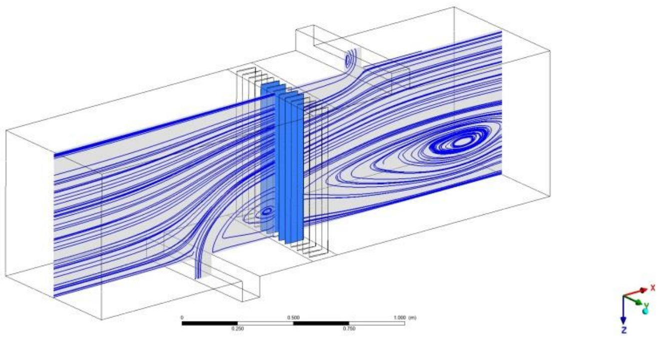

Figure 8: An example (mid-plane) of 3D CFD flow field validated against experimental data.

4 Conclusion

The experimental and numerical simulations of the flexible blade cascade in the prismatic wind tunnel were performed as part of a research project on the aeroelastic stability of a cascade influenced by a strong radial flow component. This paper strictly focuses on analyzing cascade stability through blade vibration assessment and on characterizing the wake topology behind the middle blades of the cascade.

It was shown that the cascade remains stable for any tested main tunnel flow rate. When the bypass flow is introduced, it creates cross-flow with a significant radial component and a large recirculation zone behind the blowing orifice. Under these conditions, the cascade becomes unstable and self-induced oscillations develop. While the vibration frequency stays nearly constant, the amplitude increases as the bypass flow rate rises.

Particle Image Velocimetry was used to assess the complex three-dimensional flow field around the cascade. The regularity, in terms of mean values, of the flow in the spanwise direction is immediately disrupted after the bypass flow is introduced. The velocity distribution, associated flow mass rate, and flow fluctuation activity cause substantially different flow behaviors around the cascade in each horizontal plane. The originally periodic vortex street transforms into a chaotic flow containing many energetic coherent structures of various frequencies. This phenomenon, in particular, contributes to the loss of cascade stability.

Future research will involve a detailed examination of these coherent structures using decomposition techniques, along with an evaluation of their role in transferring energy to the blades and potential attenuation mechanisms. For such analysis, the limitations of the PIV system are clear; therefore, hot-wire anemometry with a higher frequency response should be employed.

Acknowledgement

This work was supported by institutional support RVO61388998 and by the project of Czech Science Foundation No. 24-12144S "Investigation of 3D flow structures and their effects on aeroelastic stability of turbine-blade cascades using experiment and deep learning approach".

References

[1] Mambro, A., Congiu, F., Galloni, E. & Lanni, D., 2022. "Blade Drag Resistance in Windage Operating of Low Pressure Steam Turbines". Fluids, 7(12), p.372.

[2] Jutur, P., Barman, D. & Govardhan, R. N., 2022. "Low Reynolds number stall flutter of a linear cascade with large amplitudes at low reduced frequencies: Unsteady loads and flow features". Journal of Fluids and Structures, 109, 103490.

[3] Meingast, M., Kielb, R. E., Thomas, J. P., 2009. "Preliminary flutter design method for supersonic low pressure turbines". ASME Turbo Expo, 507-515.

[4] Nowinski, M. & Panovsky, J., 2000. "Flutter Mechanism in Low Pressure Turbine Blades". J. Eng. Gas Turbines Power, 122(1), 82-88.

[5] Giauque, A., Schuster, D. & Corre, Ch., 2023. "High-fidelity numerical investigation of a real gas annular cascade with experimental validation". Physics of Fluids, 35 (12): 126119.

[6] Procházka, P., Šnábl, P., Chindada, S., Prasad, Ch. S., Uruba, V. & Pešek, L., 2025. "The broad study of blade cascade under controlled torsional flutter: Dynamics of the flow and stability analysis". European Journal of Mechanics- B/Fluids, 109, 66-79.

[7] Šnábl, P., Pešek. L., Prasad, Ch. S., Procházka, P., Skála, V. & Chindada, S., to be published in 2026. "Pulse Excitation of Linear Blade Cascade Blades: Experimental Investigation and Analytical Modelling of Aeroelastic Couplings".

[8] Duda, D., Klimko, M., Milčák, P., Jeřábek, M., Uruba, V., Yanovych, V. & Žitek, P., 2024. "Wakes and secondary structures past stator wheel in test turbine VT-400 observed by PIV". European Journal of Mechanics – B/Fluids, 105, 151–163.

[9] Ramalingam, S., Duc Le, M. & Hsu, Ch. M., 2023. "Effects of axial distance on flow behaviour of continuous jet impinging on a flat surface using a finite confined nozzle". Journal of Turbulence, 25(1-3), 105-124.